CHAPTER V
RESULTS AND DISCUSSION

In this chapter, the results and discussion are classified into two major parts. Firstly, characterization of the Mo/HZSM-5 and Mo/HY catalysts by XRD, SEM, BET, XRF, UV-Visible and ^{27}Al MAS NMR is described in section 5.1. Secondly, catalytic performance of methane conversion is explained in section 5.2.

5.1 Catalyst Characterization

5.1.1 X-ray Diffraction Pattern

The X-ray diffraction patterns of relevant samples are shown in Figures 5.1 and 5.2.

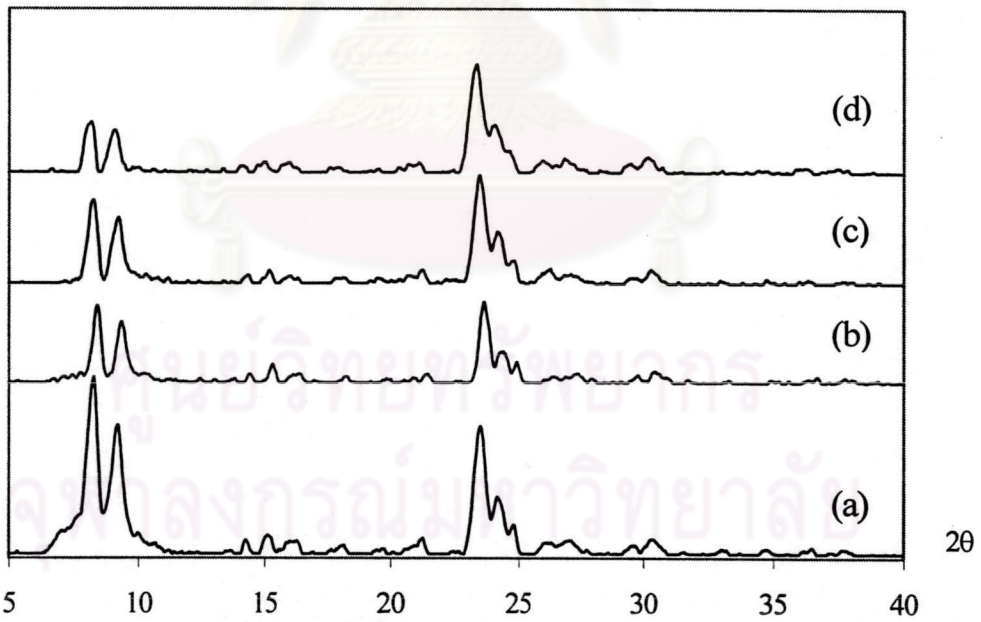

Figure 5.1 XRD patterns of various catalysts with different Mo loading. (a) HZSM-5; (b) 5%Mo/HZSM-5; (c) 8%Mo/HZSM-5; (d) 10%Mo/HZSM-5.

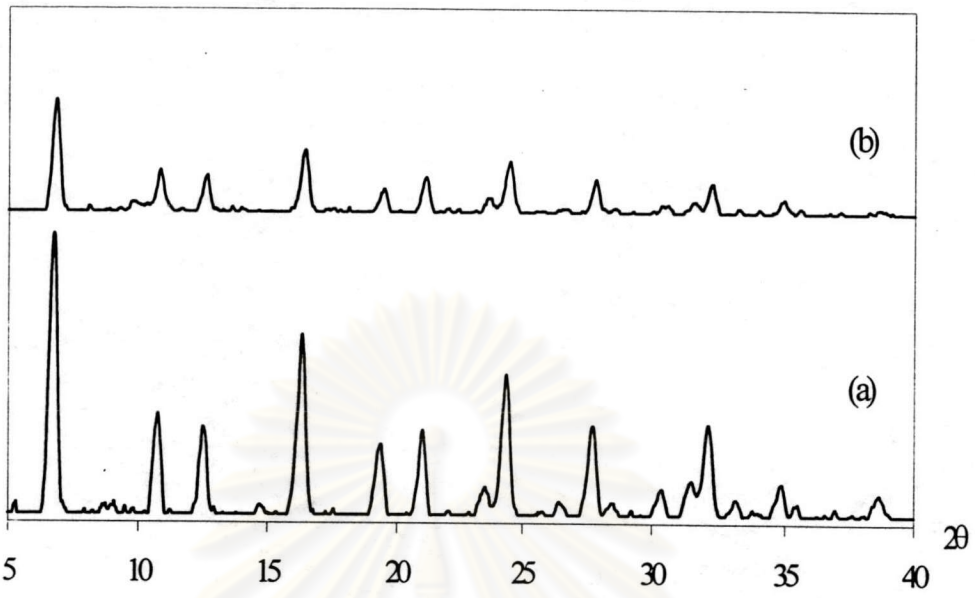

Figure 5.2 XRD patterns of (a) HY; (b) 8%Mo/HY.

Even for the 10%Mo/HZSM-5 catalyst, the pattern was similar to that of HZSM-5, only showing the characteristic peaks of HZSM-5 with the main 2θ values of about 8,9 and 23-25° as shown in Figure 5.1. No MoO_3 crystallites could be detected. This may be an indication that MoO_3 crystallites are highly dispersed on HZSM-5 and the particle size is smaller than 4 nm so that they cannot be detected by XRD technique [Jiang *et al.* (1999)]. For 8%Mo/HY catalyst, it also has the same structure as HY (Figure 5.2).

5.1.2 Morphology

Scanning Electron Microscope (SEM) photographs of the fresh and used catalysts are shown in Figures 5.3-5.7. The morphology and crystallite distributions of the fresh catalysts before and after metal loading were resemble. It was observed that the impregnation did not greatly alter the shape of crystal. Additionally, after the methane conversion reaction, the used catalyst showed the similar morphology and crystallite distributions compared with the fresh one. Average crystallite diameter of ZSM-5 was 5 μm whereas that of Y was 0.5 μm.

(a) The fresh HZSM-5 catalyst

(b) The used HZSM-5 catalyst

Figure 5.3 Scanning electron micrograph of the fresh and used HZSM-5 catalysts. (Reaction temperature of 700°C with GHSV of 2000 h^{-1})

Figure 5.4 Scanning electron micrograph of the fresh 5%Mo/HZSM-5 catalyst.

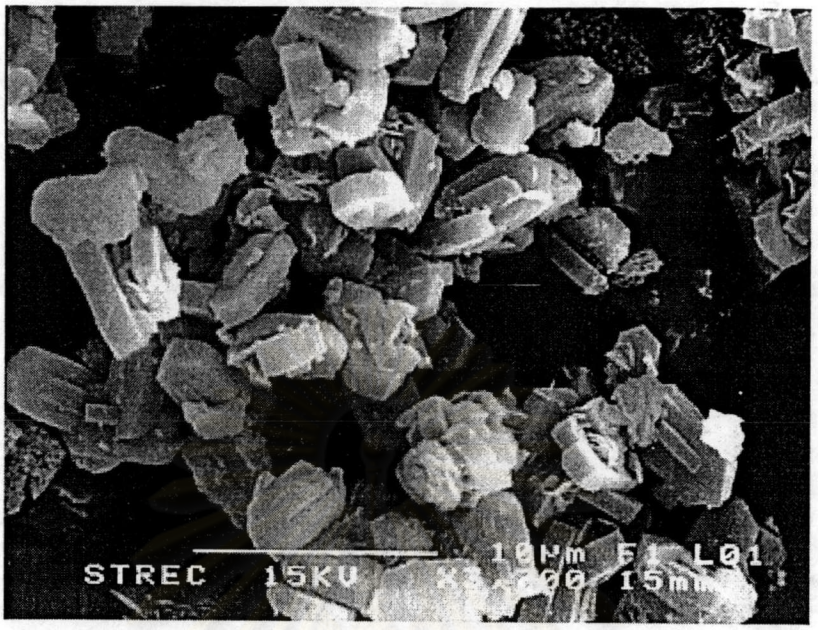

(a) The fresh 8%Mo/HZSM-5 catalyst

(b) The used 8%Mo/HZSM-5 catalyst

Figure 5.5 Scanning electron micrograph of the fresh and used 8%Mo/HZSM-5 catalysts. (Reaction temperature of 700°C with GHSV of 2000 h^{-1})

Figure 5.6 Scanning electron micrograph of the fresh 10%Mo/HZSM-5 catalyst.

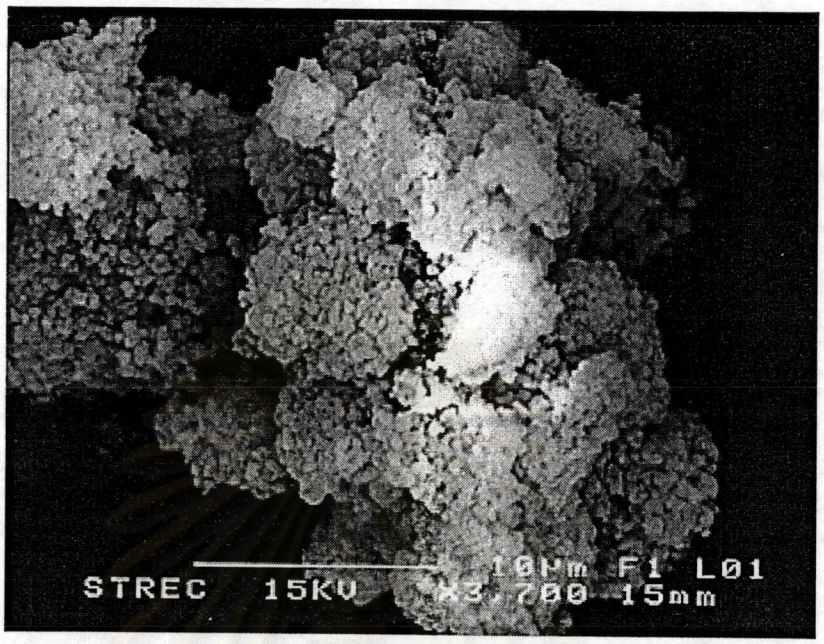

(a) The fresh 8%Mo/HY catalyst

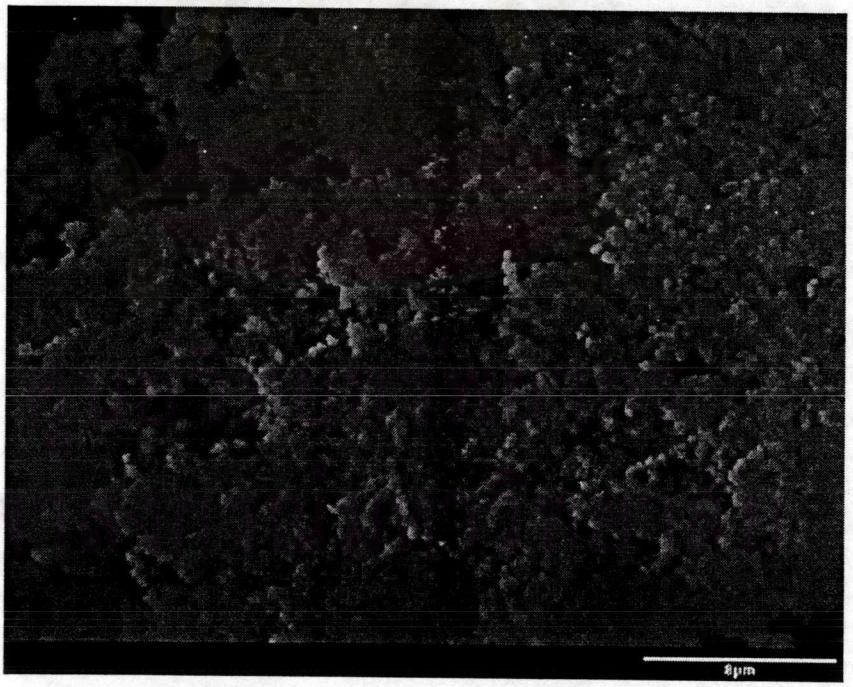

(b) The used 8%Mo/HY catalyst

Figure 5.7 Scanning electron micrograph of the fresh and used 8%Mo/HY catalysts. (Reaction temperature of 700°C with GHSV of 2000 h^{-1})

5.1.3 BET surface area

BET surface area of the various catalysts with different Mo loading is shown in Table 5.1.

Table 5.1 BET surface area of various catalysts with different Mo loading

Catalysts	BET surface area (m^2/g of catalyst)
HZSM-5	351
5%Mo/HZSM-5	310
8%Mo/HZSM-5	266
10%Mo/HZSM-5	246
HY	659
8%Mo/HY	553

From Table 5.1, the BET surface area was slightly decreased when Mo was loaded in. This introduces the channel occupation of a small amount of metal or pore mouth blockage.

5.1.4 Chemical composition

The results of quantitative analysis by XRF of molybdenum in the prepared catalysts are shown in Table 5.2. The Si/Al ratio of the commercial ZSM-5 zeolite is about 21.

Table 5.2 Mo contents in HZSM-5 and HY

% Mo loaded (by weight)	% Mo observed (by weight)
5%Mo/HZSM-5	4.22%Mo/HZSM-5
8%Mo/HZSM-5	7.30%Mo/HZSM-5
10%Mo/HZSM-5	9.24%Mo/HZSM-5
8%Mo/HY	7.8%Mo/HY

5.1.5 UV-Visible

Diffuse reflectance spectrum (DRS) of the fresh 8%Mo/HZSM-5 catalyst and the transformation of a spectrum to obtain the absorption edge energy are shown in Figures 5.8 and 5.9, respectively. As seen in Figure 5.9, intrapolation of the slope of the spectrum into x-axis resulted in the absorption edge energy at approximately 3.00 eV, which was reported in the literature as the characteristic UV absorption edge of MoO_3 [Weber (1995)]. Thus, it can be concluded that MoO_3 was obtained after impregnation and calcination

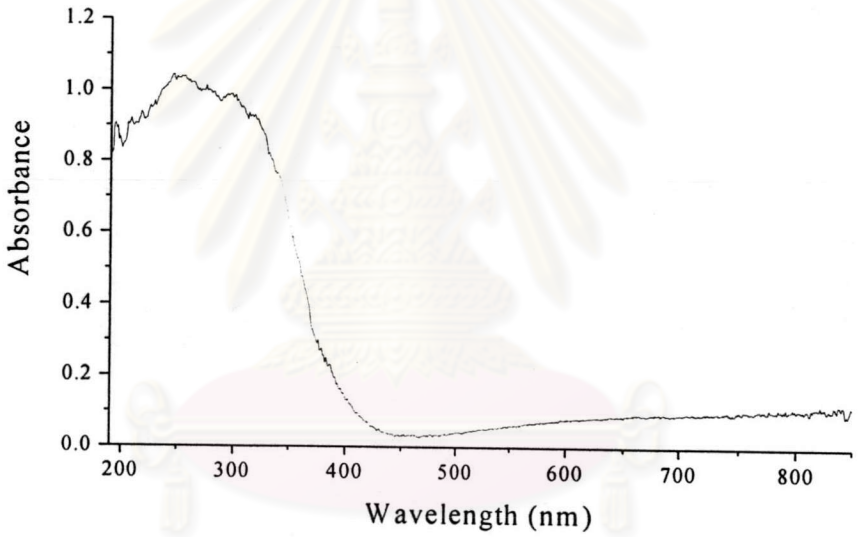

Figure 5.8 Diffuse reflectance spectrum of molybdenum oxides supported on HZSM-5.

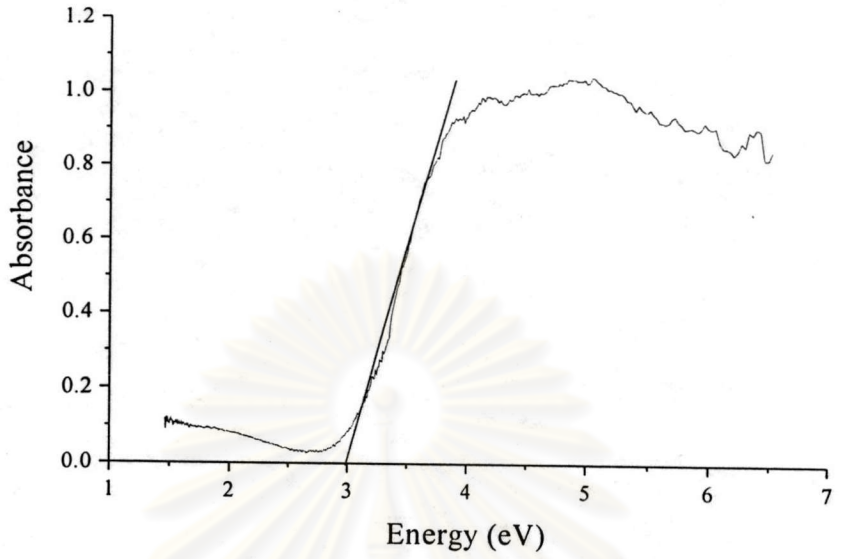

Figure 5.9 Intrapolation of the slope of the spectrum into x-axis of the transformed spectrum.

5.1.6 ^{27}Al MAS NMR

^{27}Al MAS NMR spectra of fresh and used HZSM-5 catalysts are shown in Figures 5.10 and 5.11. The methane reaction caused the appearance of the 0 ppm resonance associated with octahedrally coordinated extralattice aluminium. Loading with molybdenum also generated extralattice aluminium species (Figure 5.12). According to Figure 5.13, the intensity of extralattice aluminium species at 0 ppm increased in used 8%Mo/HZSM-5 catalyst. Additionally, a broad line can be seen at about 30 ppm due to pentacoordinated nonframework Al [Rocha *et al.* (1991), Alemany and Kirker (1986)].

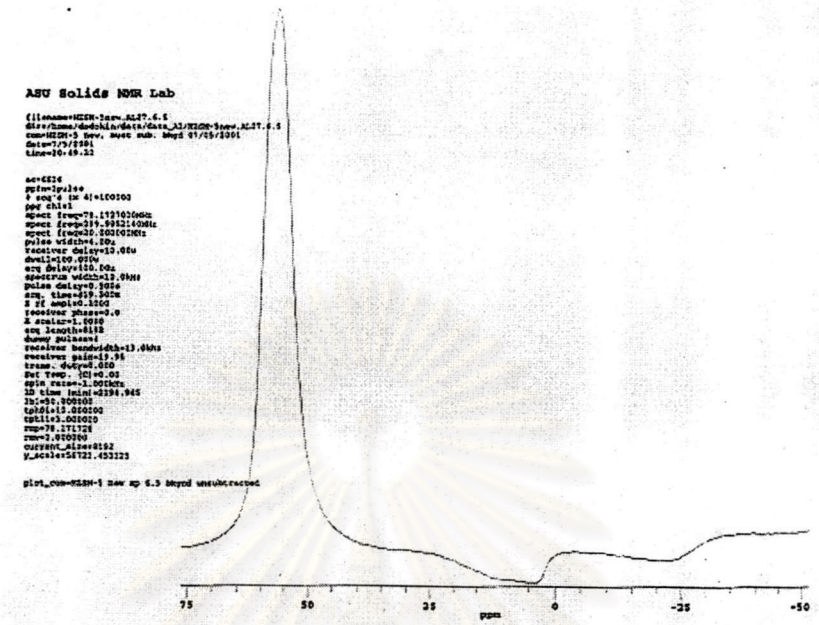

Figure 5.10 ^{27}Al MAS NMR spectrum of the fresh HZSM-5 catalyst.

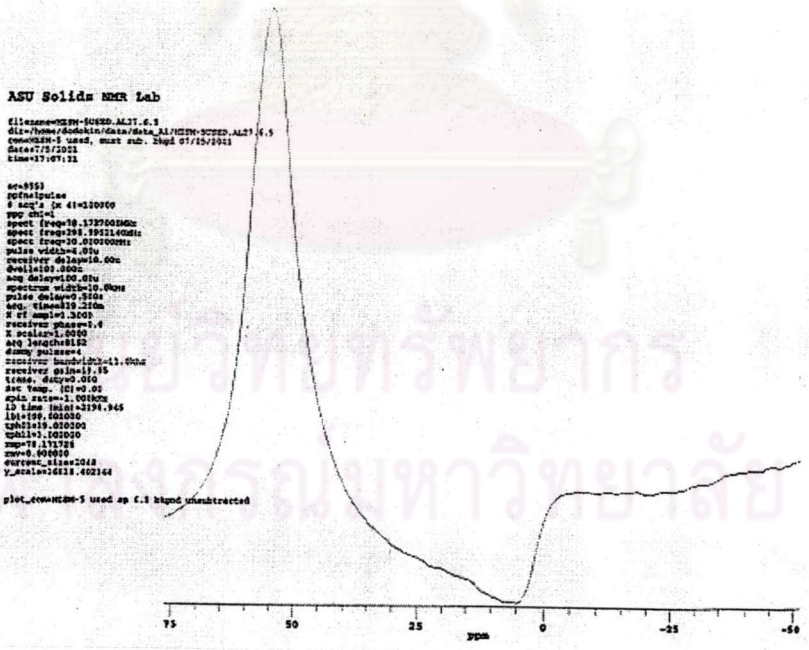

Figure 5.11 ^{27}Al MAS NMR spectrum of the used HZSM-5 catalyst. (Reaction temperature of 700°C with GHSV of 2000 h^{-1})

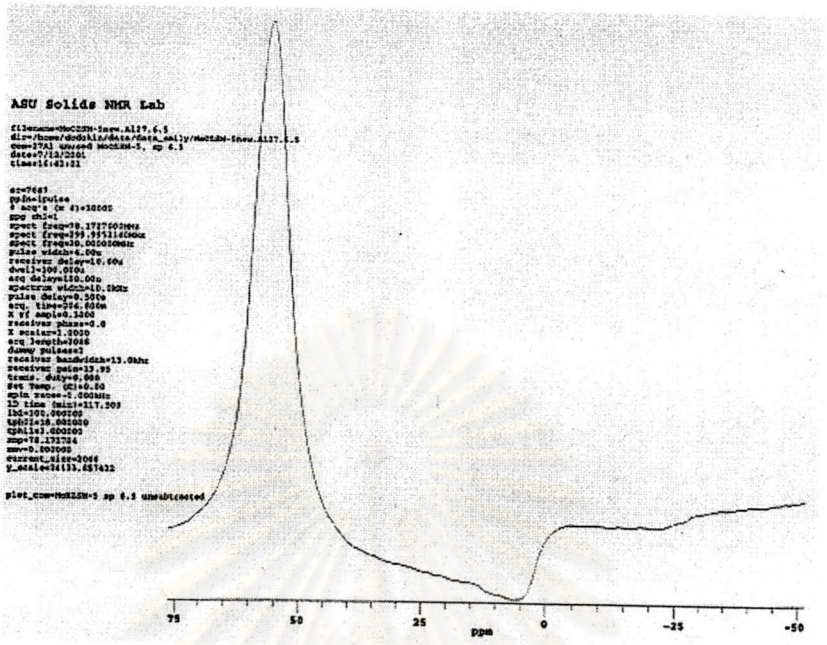

Figure 5.12 ^{27}Al MAS NMR spectrum of the fresh 8%Mo/HZSM-5 catalyst.

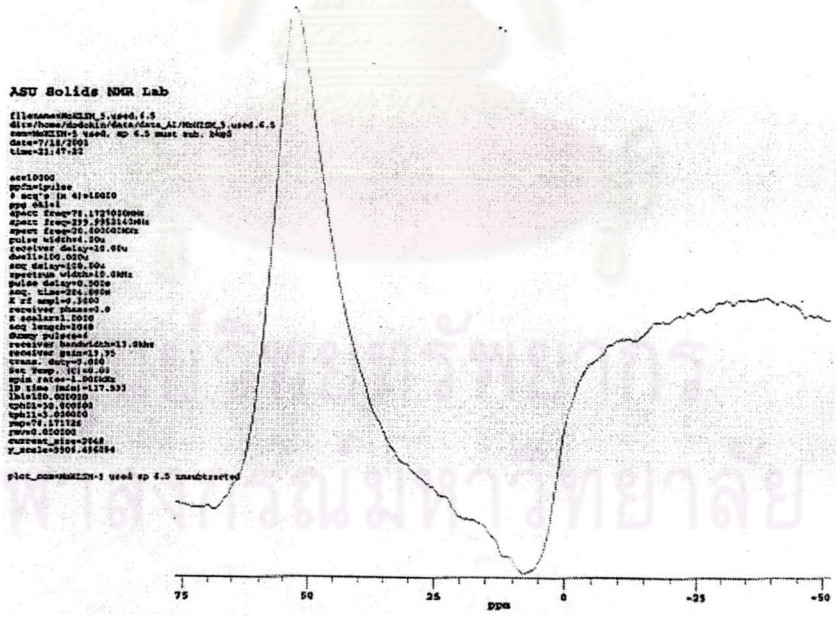

Figure 5.13 ^{27}Al MAS NMR spectrum of the used 8%Mo/HZSM-5 catalyst. (Reaction temperature of 700°C with GHSV of 2000 h^{-1})

5.2 Catalytic reaction

In this section, the catalytic performance of Mo-modified HZSM-5 and HY catalysts in the absence of oxygen is investigated.

5.2.1 Effect of the reaction temperature on the conversion of methane

The methane conversion and product distributions with time on stream at various temperatures are shown in Figures 5.14-5.17.

The reaction was carried out over 8%Mo/HZSM-5 at GHSV of 2000 h^{-1}.

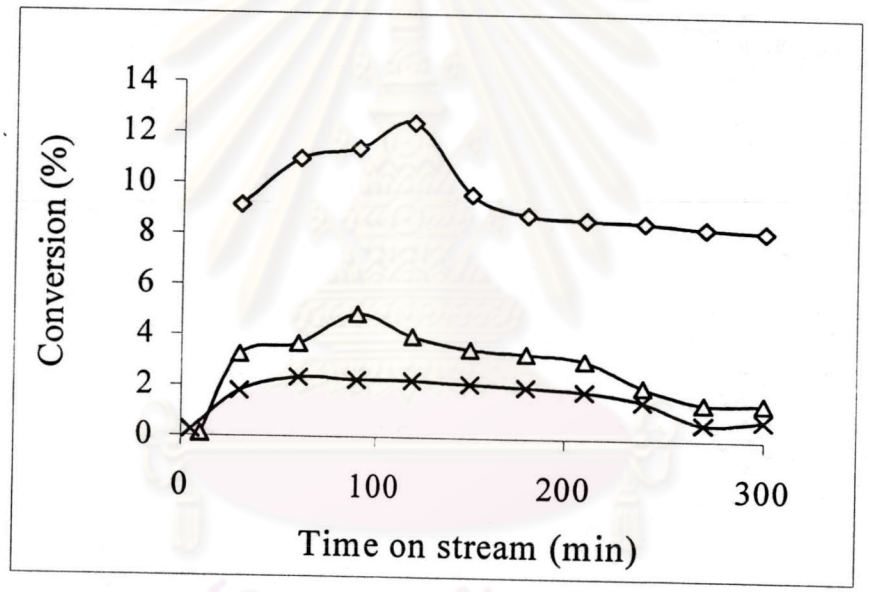

Figure 5.14 Conversion of methane on 8%Mo/HZSM-5 at different temperatures; (◊) 700°C, (Δ) 650°C, (×) 600°C.

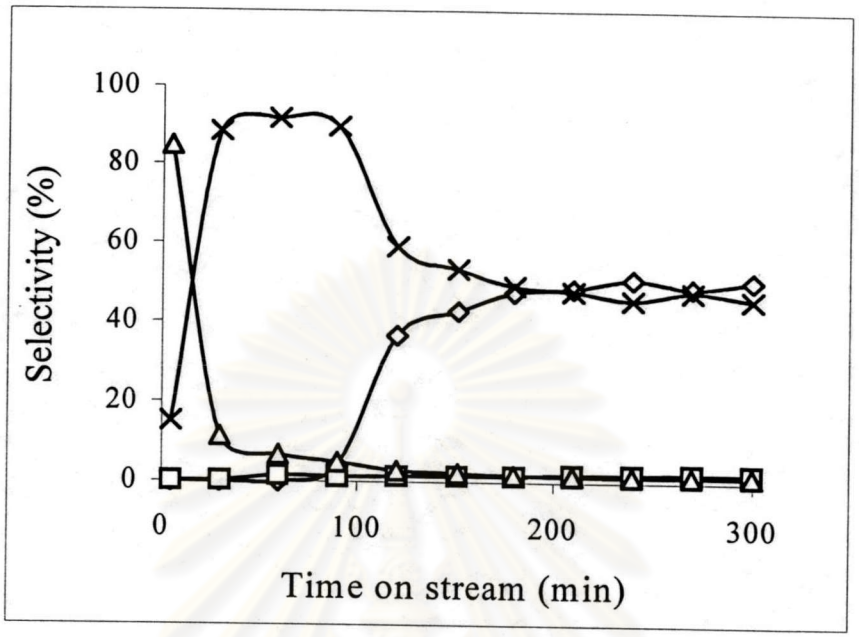

Figure 5.15 The product selectivity at reaction temperature of 600°C.
(◊) C_6H_6, (□) C_2H_4/C_2H_6, (Δ) CO_2, (×) CO.

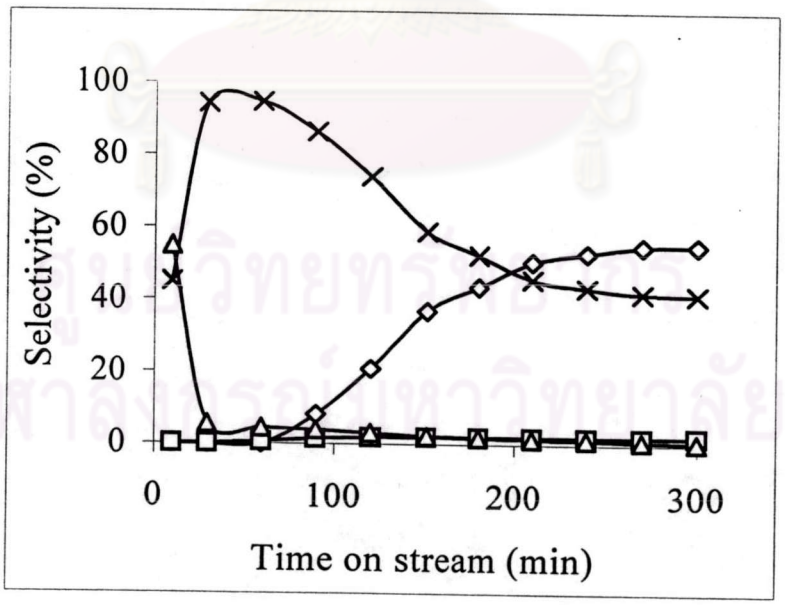

Figure 5.16 The product selectivity at reaction temperature of 650°C.
(◊) C_6H_6, (□) C_2H_4/C_2H_6, (Δ) CO_2, (×) CO.

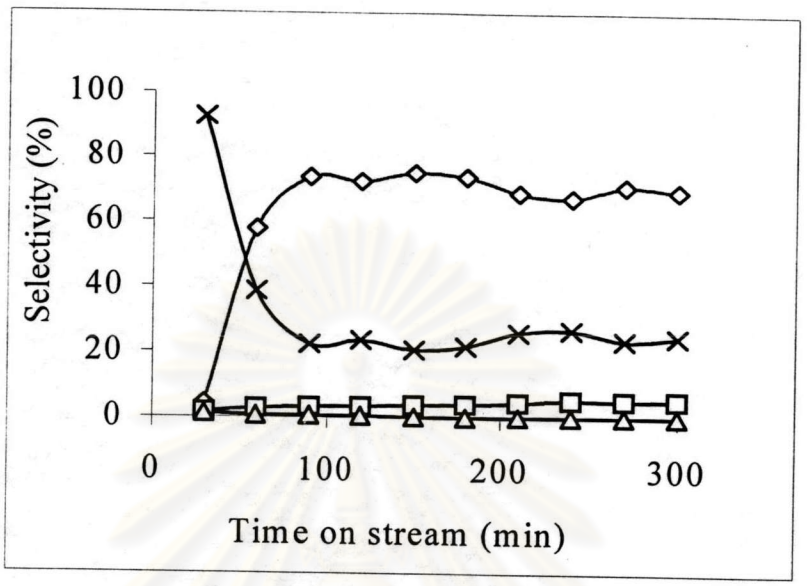

Figure 5.17 The product selectivity at reaction temperature of 700°C.
(◊) C_6H_6, (□) C_2H_4/C_2H_6, (Δ) CO_2, (×) CO.

Reaction of methane over 8%Mo/HZSM-5 was observed at different temperatures (Figure 5.14). At the beginning of the reaction, partial reduction of the catalyst predominated, as indicated by the formation of CO, CO_2 and H_2O. At 700°C, the highest methane conversion reached about 12.5%, which decayed to 8% after 2.5h. After 30 min on stream, the evolution of H_2O and CO_2 ceased, and only CO and hydrocarbons were produced. The main hydrocarbons formed were C_2H_6, C_2H_4 and C_6H_6, with minor amounts of C_3H_8 and C_7H_8 (Figures 5.15-5.17). Methane activation is difficult to be generated because methane is a thermodynamically stable product with noble gas-like configuration with very strong tetrahedral C-H bonds (435 kJ/mol) [Koerts *et al.* (1992)]. Thus, methane dissociation on MoO_3 was favorably occurred at high temperature, the molybdenum carbide species was formed which leaded to hydrocarbon product. As a result, at high temperature (700°C), methane conversion and benzene selectivity were higher than that of at low temperature (600°C) and the reaction used the shorter time to generate benzene.

In Mo/HZSM-5 samples, CO_2 and H_2O were formed as the predominant initial products. These products were formed via reactions of CH_4 with

O-atoms in MoO_3 precursors. As O-atoms in MoO_x were depleted by reduction, CO and H_2 became the predominant gas-phase products. Hydrocarbons ultimately became the catalytic products of CH_4 reactions as oxygen removal rates decreased; C_2 and aromatics (benzene) were detected in the gas phase as CO and H_2 formation rates decreased. This is in agreement with Kim *et al.*(2000), i.e., as isolated molybdenum carbide species were formed, catalytic CH_4 conversion began to produce C_2H_4 products, which were then rapidly converted to aromatics on acid sites in HZSM-5.

5.2.2 Effect of the percentage of Mo loading over HZSM-5 catalysts on the methane conversion.

The methane conversion and product distributions with time on stream in different percentage of Mo loading over HZSM-5 catalysts are shown in Figures 5.18-5.21.

The reaction was carried out at the reaction temperature of 700°C and GHSV of 2000 h^{-1}.

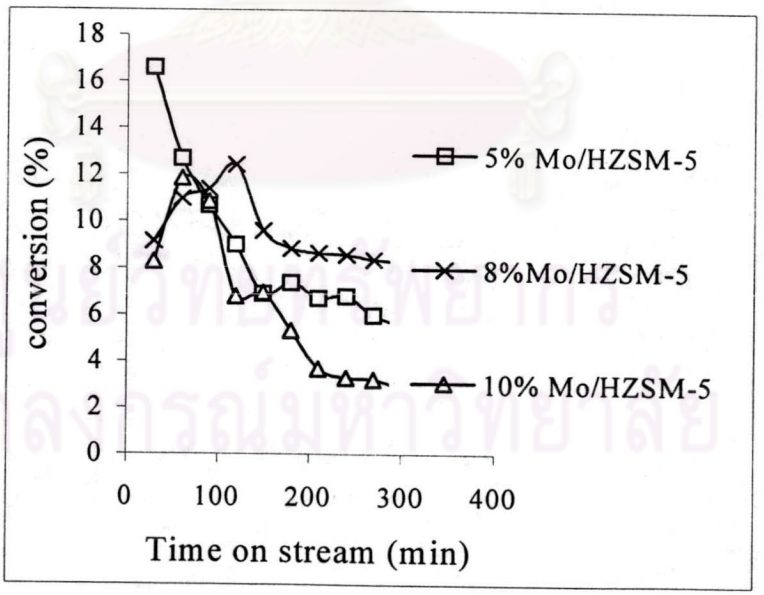

Figure 5.18 Conversion of methane at different percentage of Mo loading over HZSM-5 catalysts

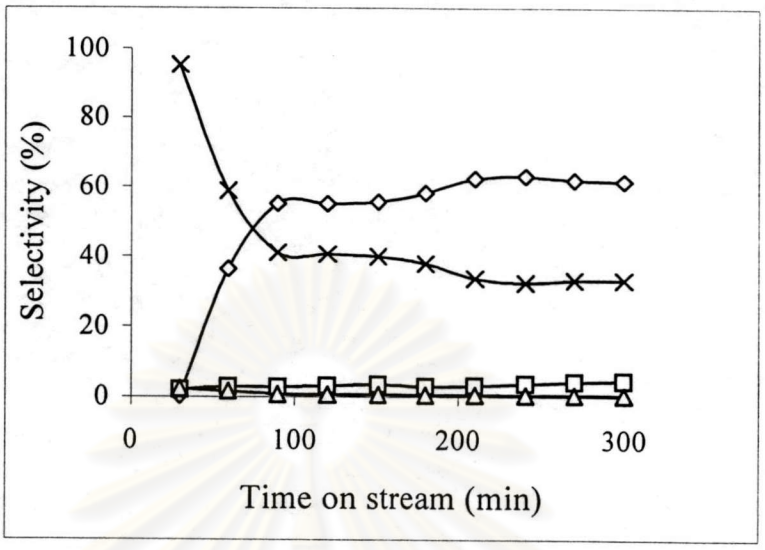

Figure 5.19 The product selectivity over 5%Mo/HZSM-5. (◊) C_6H_6, (□) C_2H_4/C_2H_6, (Δ) CO_2, (×) CO.

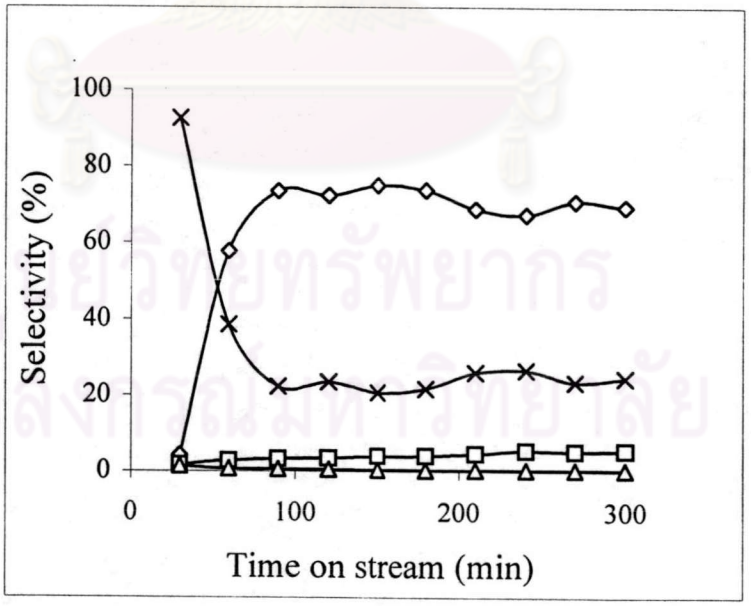

Figure 5.20 The product selectivity over 8%Mo/HZSM-5. (◊) C_6H_6, (□) C_2H_4/C_2H_6, (Δ) CO_2, (×) CO.

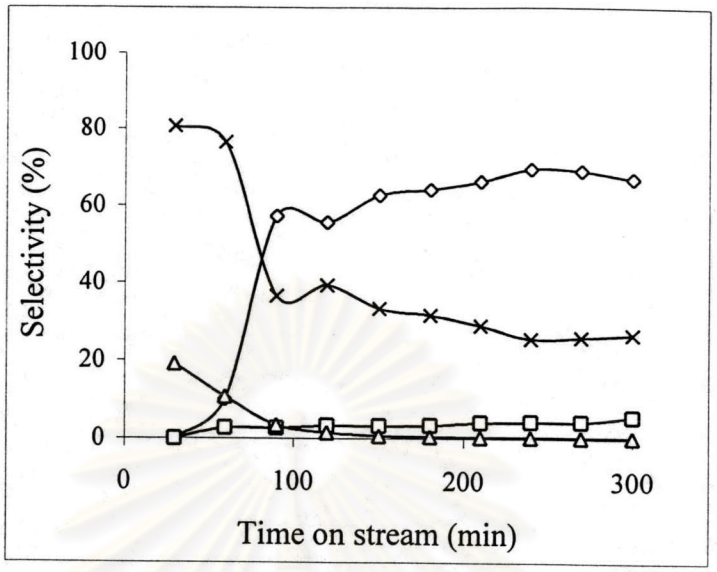

Figure 5.21 The product selectivity over 10%Mo/HZSM-5. (◊) C_6H_6, (□) C_2H_4/C_2H_6, (Δ) CO_2, (×) CO.

The similar methane conversions obtained on Mo/HZSM-5 samples. It is clearly observed that the 8%Mo/HZSM-5 gave the maximum methane conversion at 12.43% and benzene selectivity at 73%. The lower methane conversions reached on the sample with the highest Mo content (10 wt%) showing the excessive impregnation which affected to the poorly dispersed formation of MoC_x species during the reduction. The steady formation of CO can be explained by the reaction between CH_4 and H_2O.

$$CH_4 + H_2O \rightleftharpoons CO + 3H_2$$

5.2.3 Effect of the GHSV on the methane conversion.

The methane conversion and product distributions with time on stream at various GHSV are shown in Figures 5.22-5.25.

The reaction was carried out over 8%Mo/HZSM-5 at reaction temperature of 700°C.

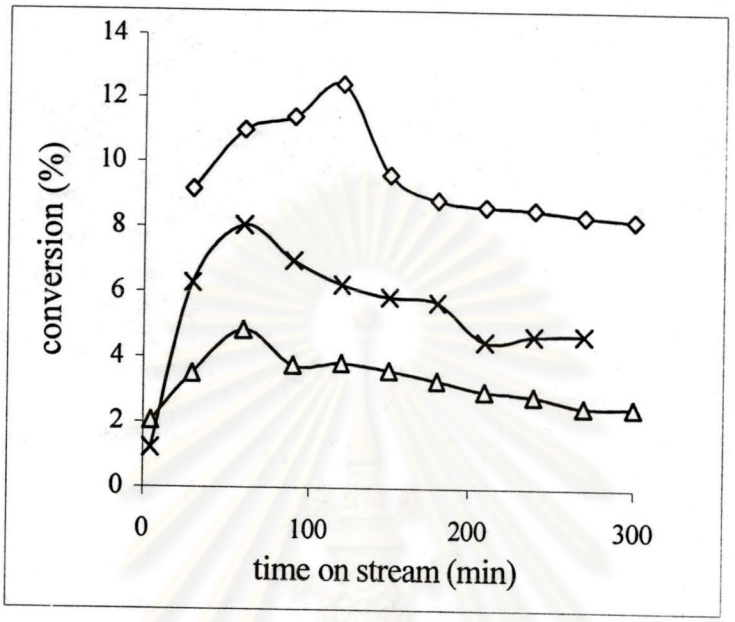

Figure 5.22 Conversion of methane on 8%Mo/HZSM-5 at different GHSV; (◊) 2000 h^{-1}, (×) 4000 h^{-1}, (Δ) 6000 h^{-1}.

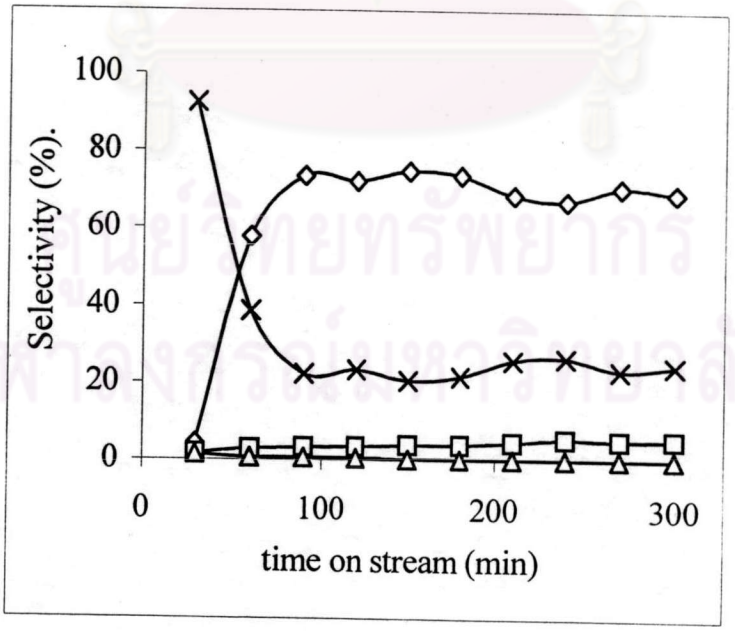

Figure 5.23 The product selectivity at GHSV of 2000 h^{-1}. (◊) C_6H_6, (□) C_2H_4/C_2H_6, (Δ) CO_2, (×) CO.

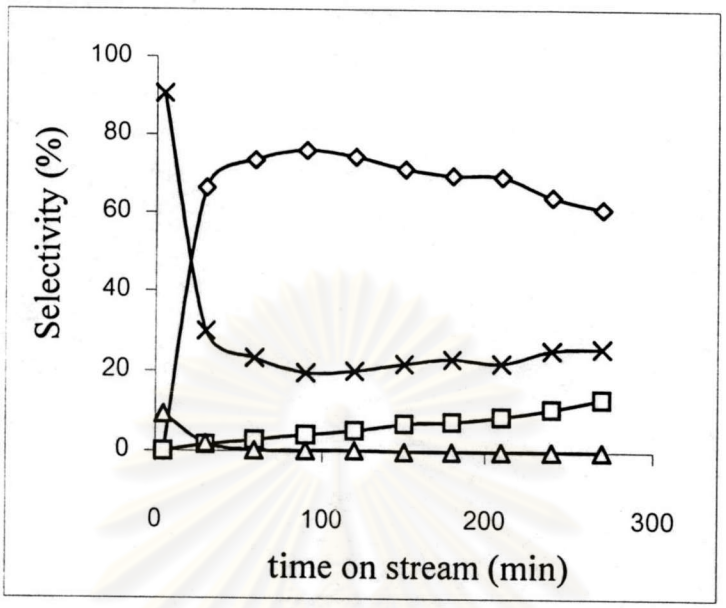

Figure 5.24 The product selectivity at GHSV of 4000 h^{-1}. (◊) C_6H_6, (□) C_2H_4/C_2H_6, (Δ) CO_2, (×) CO.

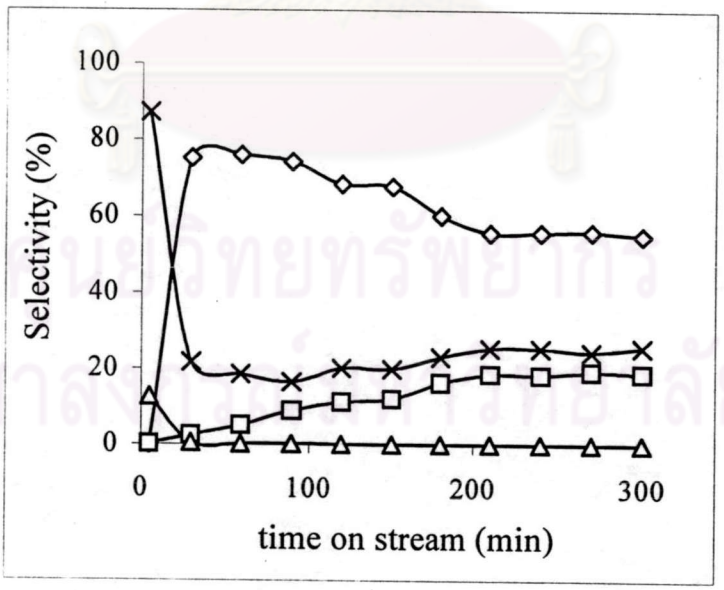

Figure 5.25 The product selectivity at GHSV of 6000 h^{-1}. (◊) C_6H_6, (□) C_2H_4/C_2H_6, (Δ) CO_2, (×) CO.

From Figures 5.22-5.25, the methane conversion increased with decreasing space velocity and the selectivity toward benzene decreased with time on stream when increased space velocity. At GHSV of 2000 h^{-1}, a benzene selectivity of 73% at a methane conversion of about 12.4% was achieved over a 8%Mo/HZSM-5 catalyst. Furthermore, the selectivity toward C_2 hydrocarbon, mainly ethylene, decreased with decreasing space velocity. This implies that ethylene was the initial product of methane activation and, that aromatics, such as benzene, are formed by subsequent reaction of ethylene.

5.2.4 Effect of the various zeolite catalysts on the methane conversion.

The methane conversion and product distributions with time on stream in various zeolite catalysts are shown in Figures 5.26-5.29.

The reaction was carried out at reaction temperature of 700°C with GHSV of 2000 h^{-1}.

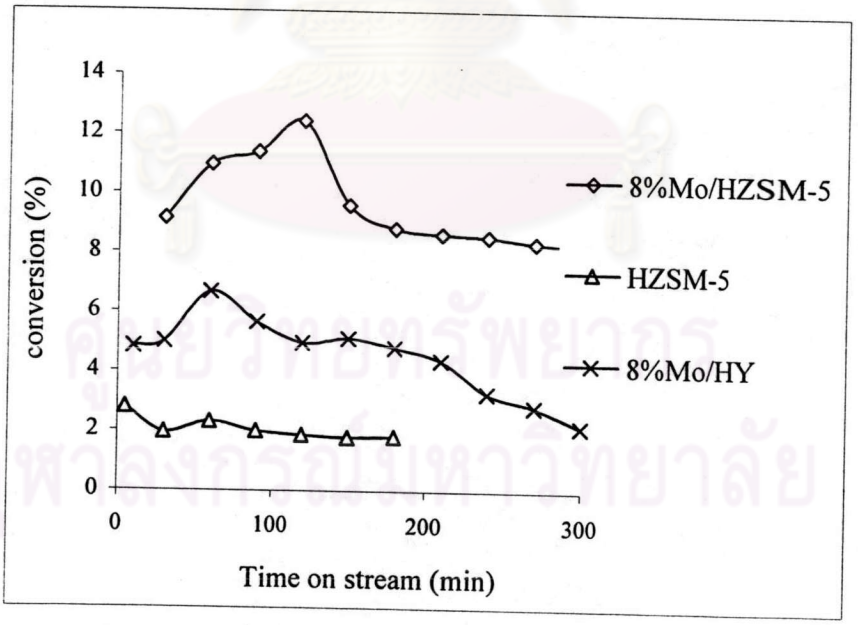

Figure 5.26 Conversion of methane on various zeolite catalysts.

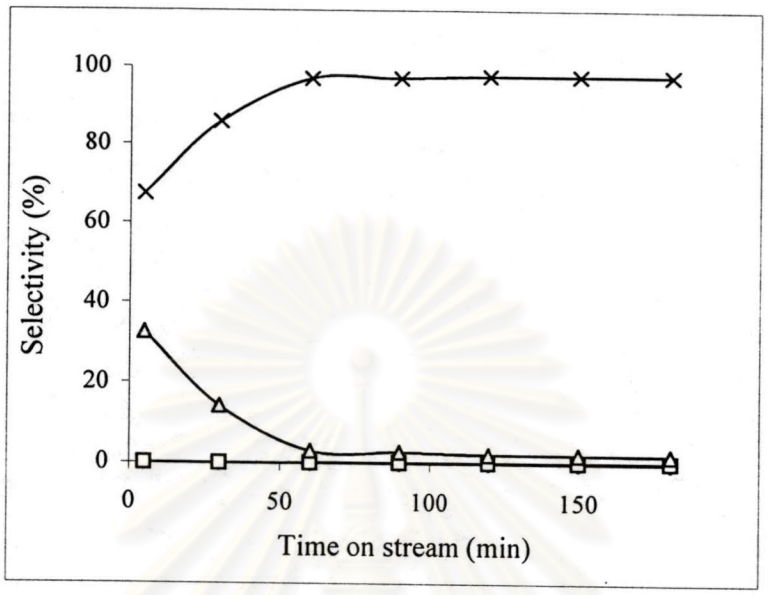

Figure 5.27 The product selectivity over HZSM-5 catalyst. (□) C_2H_4/C_2H_6, (Δ) CO_2, (×) CO.

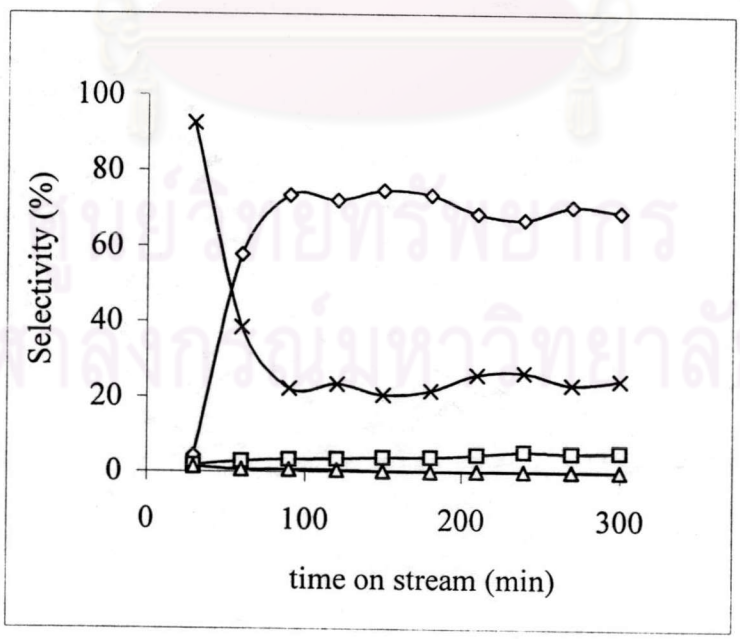

Figure 5.28 The product selectivity over 8%Mo/HZSM-5 catalyst. (◊) C_6H_6, (□) C_2H_4/C_2H_6, (Δ) CO_2, (×) CO.

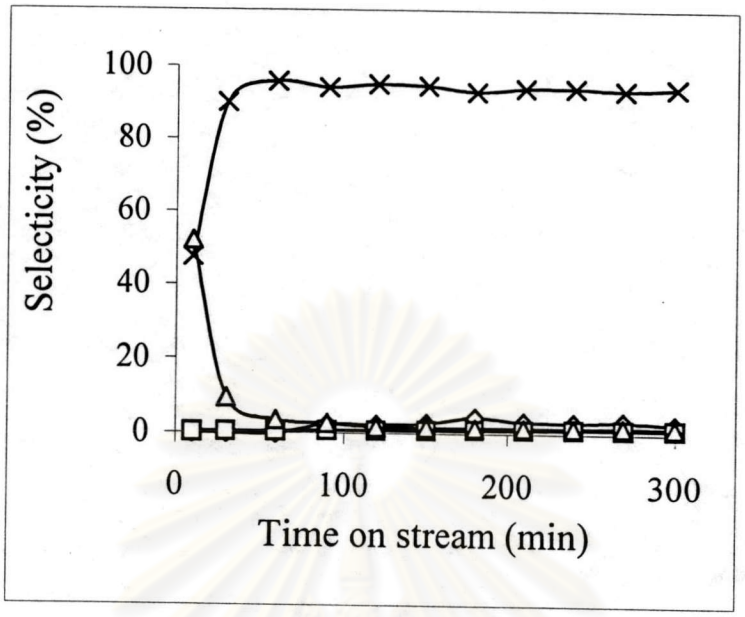

Figure 5.29 The product selectivity over 8%Mo/HY catalyst; (◊) C_6H_6, (□) C_2H_4/C_2H_6, (Δ) CO_2, (×) CO.

The methane conversion on Mo/HZSM-5, Mo/HY and HZSM-5 zeolite catalysts are summarized in Table 5.3.

Table 5.3 The conversion of methane over various zeolites at reaction temperature of 700°C with GHSV of 2000 h^{-1}

Catalyst	Conversion (%)	Selectivity(%)			
		C_6H_6	C_2	CO	CO_2
8%Mo/HZSM-5	12.43	73	3.5	23.5	0
8%Mo/HY	4.81	4.32	1.0	93.1	1.58
HZSM-5	2.32	0	0.09	96.9	3.01

Remark : Values reported at maximum hydrocarbon yield

The methane conversion and product selectivity with time on stream over various zeolite catalysts are shown in Figures 5.26-5.29 and summarized in

Table 5.3. It can be seen that Mo improved the methane conversion reaction, and Mo/HZSM-5 resulted in the relatively higher activity than Mo/HY. Therefore, zeolite structure had a significant effect on the catalytic performance. ZSM-5 possesses a pore diameter nearly equal to the dynamic diameter of a benzene molecule and has two- dimensional channel systems. Thus the effective formation and desorption of benzene formed in the channel system may minimize the formation of thermodynamically stable polyaromatic coke. This characteristic will indirectly lead to high catalytic activity. As Y zeolite is a large pore and has three-dimensional structure, this structure is advantageous to generation of condensed ring aromatics type deposited carbon. This blocks the channel rapidly, and also causes low selectivity to aromatics and even no aromatics [Zhang *et al.* (1998)].

From Figures 5.27-5.29, it was observed that the selectivity for CO was constant with time. The methane conversion in the absence of oxygen on HZSM-5 catalyst at high temperature generated CO because of the reaction between methane and oxygen in zeolite framework. It can be seen from Figures 5.10 and 5.11 that the methane conversion generated the extralattice aluminium species, implying some parts of zeolite framework were destroyed. For 8%Mo/HZSM-5 catalysts, CO was probably formed via reaction of methane with O-atoms in MoO_3 precursors and with O-atoms in zeolite framework. Consistent with ^{27}Al MAS NMR spectra in Figures 5.12 and 5.13, the intensity of extra-framework aluminium in used 8%Mo/HZSM-5 catalyst increased comparing with the fresh one. These results showed some structural degradation of the zeolite during methane conversion reaction.

In this study, Mo/HZSM-5 catalysts were prepared by incipient wetness impregnation of NH_4ZSM-5 with ammonium heptamolybdate aqueous solution [AHM; $(NH_4)_6Mo_7O_{24}.4H_2O$], followed by treatment in air at 500°C. Large aqueous molybdate ions do not exchange directly onto HZSM-5 cation exchange sites during impregnation. AHM decomposed in air between 227-377°C to form MoO_3 crystallites on external zeolite surface [Wang *et al.* (1996), Liu *et al.* (1997)]. At 500°C, MoO_3 crystallites dispersed on external ZSM-5, and ultimately migrate and exchange within zeolite channels [Xu *et al.* (1995)]. Iglesia *et al.* (1999) pointed out that the isolated MoO_x species migrate into ZSM-5 channels via vapor or surface diffusion and then could further react with H^+ atoms at exchange sites to form $(MoO_2(OH))^+$ species, which can condense with another one to form a $(Mo_2O_5)^{2+}$ dimer and H_2O :

$$2MoO_3 + 2(AlOSi)H \longrightarrow (AlOSi)Mo_2O_5(AlOSi) + H_2O$$

The $Mo_2O_5^{2+}$ species on $(AlOSi)Mo_2O_5(AlOSi)$ have ditetrahedral structures. This $Mo_2O_5^{2+}$ species can be reduced to form the active MoC_x complex during the initial stages of methane conversion reactions.

$$(AlOSi)MoO_x + CH_4 \longrightarrow (AlOSi)MoC_x + H_2O$$

MoC_x sites convert CH_4 into ethane and ethylene, which then react to form C_6-C_{10} aromatics on acid sites via rapid oligomerization, cracking and cyclization reactions.

The activation reaction sequence is proposed by Zhou *et al.* (2000) as follows:

$$CH_4 + MoC_x/HZSM\text{-}5 \longrightarrow H_2C^+{-}MoC_x/HZSM\text{-}5 + H_2$$
$$CH_4 + H_2C^+{-}MoC_x/HZSM\text{-}5 \longrightarrow H_2C^+{-}H_2C{-}MoC_x/HZSM\text{-}5 + H_2$$

The terminal C_2H_4 adsorbed on the catalyst can be liberated:

$$H_2C^+{-}H_2C{-}MoC_x/HZSM\text{-}5 \longrightarrow C_2H_4 + Mo^+C_x/HZSM\text{-}5$$

The formation of H_2 is probably the first irreversible step (or steps) and the driving force up to this stage of the reaction. The transient product C_2H_4 is tuned and encouraged to further aromatize to benzene in the pore of the ZSM-5 zeolite under appropriate conditions:

$$3C_2H_4 \longrightarrow C_6H_6 + 3H_2$$

Alternatively, $H_2C^+ - H_2C - MoC_x/HZSM\text{-}5$ could react with methane via an oligomerization process:

$$CH_4 + H_2C^+{-}(H_2C)_n{-}MoC_x/HZSM\text{-}5 \longrightarrow H_2C^+{-}(H_2C)_{n+1}{-}MoC_x/HZSM\text{-}5 + H_2$$

The long-chain complex is capable of aromatization under assistance of the three-dimensional structure of the pore structure:

$$H_2C^+{-}(H_2C)_5{-}MoC_x/HZSM\text{-}5 \longrightarrow C_6H_6 + MoC_x/HZSM\text{-}5 + 3H_2$$

The channel structure of ZSM-5 is the geometric factor to meet the critical requirement of aromatization.